Engineering Transactions, **68**(2): 177–198, 2020, doi: 10.24423/EngTrans.925.20200601
Polish Academy of Sciences • Institute of Fundamental Technological Research (IPPT PAN)
Université de Lorraine • Poznan University of Technology

Research Paper

Navier Slip Condition on Time-Dependent Radiating Nanofluid with the Soret Effect

Sangapatnam SUNEETHA[1)], Ketineni SUBBARAYUDU[1)]
Lalahamed WAHIDUNNISA[1)], Polu Bala Anki REDDY[2)*]

[1)] *Department of Applied Mathematics*
Yogi Vemana University
Kadapa-516003, Andhra Pradesh, India

[2)] *Department of Mathematics*
School of Advanced Sciences, VIT University
Vellore-632014, India
*Corresponding Author e-mail: pbarmaths@gmail.com

This work concentrates on the study of the two-dimensional hydromagnetic flow of nanofluids over an suddenly started nonlinear stretching sheet in the presence of radiation and dissipation. The Soret effect and heat generation are also taken into consideration. The transformed ordinary differential equations (ODEs) are solved numerically via the MATLAB RK4S approach bvp4c solver with the assistance of similarity variables. The effects of various parameters are explored and shown in graphs and tables. It is noted that the concentration increases as the Soret number increases within the boundary layer. An increase in velocity slip decreases the velocity and a reverse effect is observed for temperature. This model has significance in different areas such as polymer chemical and metallurgical industries, and other fields that use the latest technology and thermo-processed materials such as metallic and glass sheets.

Key words: nanofluids; MHD; thermal radiation; viscous dissipation; heat generation; Soret effect.

Notations

a – constant parameter [s^{-1}],
A – unsteadiness parameter,
B – magnetic field [$kg/(s^2 \cdot A)$],
B_0 – constant magnetic field [$kg/(s^2 \cdot A)$],
C – nanoparticle concentration,
C_∞ – concentration of nanoparticle in the free stream,
C_{f_X} – local skin friction coefficient,
C_w – concentration of nanoparticle at the wall of the sheet,
D_B – Brownian diffusion coefficient [m^2/s],
D_T – thermophoretic diffusion coefficient [m^2/s],

Ec – Eckert number,
f – dimensionless stream function,
h – element size [m],
k – thermal conductivity [W/(m · K)],
k^* – Rosseland mean absorption coefficient [m^{-1}],
Le – Lewis number,
M – magnetic parameter,
n – stretching index,
N – velocity slip factor [m],
N_1 – initial velocity slip factor [m],
Nb – Brownian motion parameter,
Nt – thermophoresis parameter,
Nu_X – local Nusselt number,
Pr – Prandtl number,
$\mathrm{Pr}_{\mathrm{eff}}$ – effective Prandtl number,
Q – heat source/sink parameter,
q_m – wall mass flux [kg/(m^2 · s)],
q_r – radiative heat flux [W/m^2],
q_w – wall heat flux [W/m^2],
R – radiation parameter,
Re_X – local Reynolds number,
Sh_X – local Sherwood number,
Sr – Soret number,
T – temperature [K],
t – time [s],
T_1 – temperature in free stream [K],
u – velocity along x-direction [m/s],
v – velocity along y-direction [m/s].

Greek Symbols

$(\rho c)_f$ – specific heat capacity of the base fluid [J/K],
α_m – thermal diffusivity [m^2/s],
γ – velocity slip parameter,
η – similarity variable,
θ – dimensionless temperature,
λ – constant with dimension reciprocal of time [s^{-1}],
μ – dynamic viscosity [kg/(m · s)],
ν – coefficient of kinematic viscosity [m^2/s],
ρ – density [kg/m^3],
σ – electrical conductivity [s/m],
σ^* – Boltzmann constant [W/(m^2 · K^4)],
τ – specific heat capacity of nanoparticles/specific heat capacity of fluid,
τ_w – wall shear stress [kg/(m · s^2)],
ϕ – dimensionless nanoparticle concentration,
ψ – stream function [m^2 · s].

1. Introduction

The fluids like H_2O, $C_2H_6O_2$ and engine oil are poor conductors of heat transfer. The thermal conductivities of such fluids called host fluids can be improved by adding nanometer-sized particles known as nanoparticles. Such fluids are called nanofluids and were first introduced by Choi and Eastman [1]. The nanoparticles are made from distinct substances like metals: Cu, Hg, Au, Ti, Ag, etc., and non-metals: CuO, SiO_2, Al_2O_3, TiO_2, etc. The collective research of heat and mass transfer in nanofluid has numerous engineering and biomedical applications, including microelectronics, hybrid-powered engines, pharmaceutical processes, cancer therapy, domestic refrigerator, and heat exchanger [2–4].

Many studies are confined to stretching the plate linearly. It is striking that the heat transfer over a nonlinear surface has many industrial applications such as manufacturing of plastic sheets in aerodynamics, metallic plate condensing in a cooling bath, and manufacturing of a dye polymer sheet. While manufacturing, the sheet is stretched accordingly to the required thickness. The final products are influenced by the rate of stretching, cooling process rate, and procedure of stretching. The flow due to the stretching of a flat plane was initially examined by Crane [5]. The study of fluid moving over a nonlinear stretching sheet, in different situations, has been presented by various researchers [6–10].

In fluid dynamics, the influence of the magnetic field over a stretching plane has significant applications in engineering and industry, such as geophysics, in controlling heat transfers of different nanofluids, in paper production and so forth. Hamad *et al.* [11] obtained results with magnetohydrodynamics (MHD) over an infinite flat plate. Bala Anki Reddy *et al.* [12] analyzed the MHD flow of Maxwell nanofluid over an exponentially stretching plane. A numerical model with nanofluid over a nonlinear stretching/shrinking sheet was developed by Daniel *et al.* [13]. The authors observed that the nanoparticle concentration increases with mass convective conditions. Hayat *et al.* [14] elaborated on the flow of Powell-Eyring magnetic nanofluid over a nonlinear stretched sheet with changeable thickness, and reported that the surface drag coefficient increases for improved values of the magnetic parameter.

In the thermal radiation process, heat energy is released as the type of electromagnetic waves from a radiated surface in 360°. When high temperatures are encountered, the thermal radiation effect becomes very important. In space technology, thermal radiation plays a pivotal role in operating the devices at extremely high-temperature levels. A few latest investigations considering the impacts of thermal radiation are given in [15–19].

The distribution of temperatures is changed by viscous dissipation, which is a source for energy and impinges on the heat transfer rate. The viscous dissipation plays a key role in geophysical flows and assured industrial operations,

and it is depicted by the Eckert number. The study of the nonlinear stretching sheet, for various problems of fluid flow, has been conducted by different authors [20, 21]. KHAN *et al.* [22] considered the effect of dissipation on the axisymmetric squeezing flow of copper nanoparticles in the base fluids (water and kerosene).

In the previous studies, discussions were restricted to conventional boundary conditions without slip. However, in many practical appliances such as micro and nano-scaled devices, velocity slip and temperature slip play a vital role. To demonstrate the slip nature of liquid on the solid surface, NAVIER [23], in 1823, was the first to introduce the fluid velocity component which was tangential to the solid surface and proportional to the shear stress on the solid interface. Additionally, he recommended that the slip velocity and the shear stress are proportional at the wall. The slip effect over a stretching surface with nanofluid was conducted by SHAW *et al.* [24]. OYELAKIN *et al.* [25] examined the convective and slip effect on a time-dependent Casson nanofluid. KHAN and SULTAN [26] and KHAN *et al.* [27] studied the effects of slip conditions on a rotating disk with different fluids.

The impact of heat generation or absorption in flowing fluids is very significant in chemical reactions and fluid separation. Generally, heat generation modifies the temperature in the fluids, which affects the deposition rate of particles in the system, for example, electronic chips, nuclear reactors, semiconductors, etc. Some important studies in connection to heat impact are presented in [28–30].

In a system with flowing fluid, an important thermodynamic trend/phenomena is called the Soret effect, in which dissimilar particles react in different ways to altering temperatures. The mass flux can be generated both by the concentration and temperature gradients. Mass fluxes produced by temperature gradients are called the Soret effect. In 1879, Charles Soret, a Swiss chemist, examined this effect specifically in the Earth's gravity. In his experiment, he filled a tube with salt solution. One end of this tube was placed into a hot bath and the other one was in a cold bath. At the end of this experiment, he found that more salt was concentrated at the cold end than at the hot end. This effect plays a significant role in the operation of solar ponds, microstructure of seas and oceans, and the transportation across biological membranes induced by small thermal gradients in living creatures. The latter one is an essential factor in biological systems. Although the Soret effect is quite small, it is used in the separation of components in mixtures. Generally, this effect is ignored in mass transfer processes and its magnitude is very small when compared with the effect of Fick's law. Thermophoresis or Soret effects are noteworthy when there exists a difference in the density in the flow field, as in the case of geo-sciences and hydrological fluid flow situation. Additionally, this effect can be highly relevant on design and operation of dryers. ECKERT and DRAKE [31] highlighted the Soret effect related to the parting of isotopes and in the combination of gases with small

molecular weight (H_2, He) and the average molecular weight (N_2, air). Based on this, many researchers have applied the Soret effect to various mass transfer problems. YIRGA and SHANKAR [32] studied the MHD flow and heat transfer of nanofluids through a porous media due to a stretching sheet with viscous dissipation and chemical reaction effects. REDDY *et al.* [33] studied the impact of the Soret effect on stagnation-point flow past a sheet in a nanofluid with non-Darcy porous medium. MISHRA *et al.* [34] presented the chemical reaction effect on micropolar fluid along a stretching sheet with the Soret effect.

Prompted by the above literature survey and the extensive engineering and industrial uses, it is time to explore the influence of the Soret effect on electrically conducting natural convection flow of radiating dissipative nanofluid over a nonlinearly stretching sheet with Navier slip and heat generation. The transformed ODEs are solved numerically using the MATLAB RK4S approach bvp4c solver with the help of similarity variables. The influence of various parameters is explored and depicted through graphs and tables. Such flow problems may come up in quite a few industrial processes: coolant application, manufacture of ceramics and glassware, nano-drug delivery, cooling of microchip, polymer production, etc.

2. Mathematical analysis

Consider a laminar incompressible flow of MHD radiating nanofluid over a nonlinear stretching sheet. The problem is characterized by dissipation and the Soret effect, which are used to study it. The sheet stretches along the X-axis and then it raises along the Y-axis. The Reynolds number is measured as one minute, so the induced magnetic field is tiny. The magnetic flux B is applied upright to the sheet. When the fluid is stationary at $t \leq 0$, the temperature of the sheet and concentration of the nanoparticle are T_w and C_w, respectively. When $t > 0$, the sheet stretches constantly with a velocity $u_w(X,t) = \frac{aX^n}{1-\lambda t}$, where a – constant, n – nonlinear stretching index, and λ – constant with dimension reciprocal of time. The temperature and concentration of the ambient fluid are T_∞ and C_∞, in that order. A transverse time dependent magnetic field of variable intensity ($B(X,t)$) is imposed parallel to the Y-axis. A geometrical model of the present physical problem is displayed in Fig. 1. The Reynolds number is understood to be small and it is produced by the magnetic field in a fluid flow [35].

According to Prandtl's theory of boundary layer, the flow assumptions made above can be written in the following form [36–38]:

$$\frac{\partial u}{\partial X} + \frac{\partial v}{\partial Y} = 0, \tag{2.1}$$

$$\frac{\partial u}{\partial t} + u\frac{\partial u}{\partial X} + v\frac{\partial u}{\partial Y} = \nu\frac{\partial^2 u}{\partial Y^2} - \frac{\sigma B^2 u}{\rho}, \tag{2.2}$$

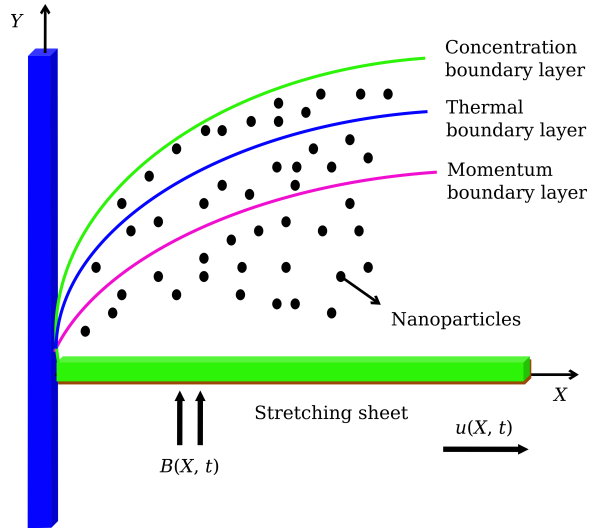

FIG. 1. Model representing the flow problem.

$$(2.3)\quad \frac{\partial T}{\partial t}+u\frac{\partial T}{\partial X}+v\frac{\partial T}{\partial Y} = \alpha_m\frac{\partial^2 T}{\partial Y^2}+\tau\left[D_B\frac{\partial C}{\partial Y}\frac{\partial T}{\partial Y}+\frac{D_T}{T_\infty}\left(\frac{\partial T}{\partial Y}\right)^2\right] -\frac{1}{(\rho c)_f}\frac{\partial q_r}{\partial Y}+\frac{Q_0}{\rho c_p}(T-T_\infty)+\frac{\mu}{\rho c_p}\left(\frac{\partial u}{\partial Y}\right)^2,$$

$$(2.4)\quad \frac{\partial C}{\partial t}+u\frac{\partial C}{\partial X}+v\frac{\partial C}{\partial Y} = D_B\frac{\partial^2 C}{\partial Y^2}+\frac{D_T}{T_\infty}\frac{\partial^2 T}{\partial Y^2}+\frac{D_m k_T}{T_m}\frac{\partial^2 T}{\partial Y^2}.$$

For static fluid, the primary and border conditions are specified as:

$$(2.5)\quad (t\le 0): u=0,\ v=0,\ T=T_w,\ C=C_w,$$

u and v are functions of X and t

$$(2.6)\quad t>0: \begin{cases} u=u_w+u_{\text{slip}}=\dfrac{aX^n}{1-\lambda t}+N\mu\dfrac{\partial u}{\partial Y},\ v=0,\ T=T_w,\ C=C_w,\ \text{at } Y=0,\\ u\to 0,\ T\to T_\infty,\ C\to C_\infty \text{ as } Y\to\infty. \end{cases}$$

By using the Rosseland approximation for an optically thick fluid, the radiative heat flux q_r is

$$(2.7)\quad q_r=-\frac{4\sigma}{3k}\frac{\partial T^4}{\partial Y},$$

linearizing the nonlinear term T^4 in Eq. (2.7) with Taylor's series, by assuming a small variation between the fluid temperature within the boundary layer and ambient fluid temperature, retaining terms up to first order only, T^4 is denoted as:

$$T^4 \cong 4T_\infty^3 T - 3T_\infty^4. \tag{2.8}$$

Equation (2.3), after including Eqs (2.7) and (2.8), is given as:

$$\frac{\partial T}{\partial t} + u\frac{\partial T}{\partial X} + v\frac{\partial T}{\partial Y} = \alpha_m \frac{\partial^2 T}{\partial Y^2} + \tau\left[D_B \frac{\partial C}{\partial Y}\frac{\partial T}{\partial Y} + \frac{D_T}{T_\infty}\left(\frac{\partial T}{\partial Y}\right)^2\right] + \frac{1}{(\rho c)_f}\frac{16\sigma^* T_\infty^3}{3k^*}\frac{\partial^2 T}{\partial Y^2} + \frac{Q_0}{\rho c_p}(T - T_\infty) + \frac{\mu}{\rho c_p}(\frac{\partial u}{\partial Y})^2. \tag{2.9}$$

The following are used to convert PDEs (2.2), (2.4), and (2.9) with boundary conditions (2.5) and (2.6) into ODEs:

$$\eta = y\sqrt{\frac{u_w(X,t)}{\nu X}}, \qquad \psi = \sqrt{\nu X u_w(X,t)}f(\eta),$$
$$\theta(\eta) = \frac{T - T_\infty}{T_w - T_\infty}, \qquad \phi(\eta) = \frac{C - C_\infty}{C_w - C_\infty}, \qquad u(X,t) = u_w(X,t)f'(\eta), \tag{2.10}$$
$$v(X,t) = -\sqrt{\frac{u_w(X,t)\nu}{X}}\left(\frac{n+1}{2}f(\eta) + \frac{n-1}{2}\eta f'(\eta)\right).$$

The velocity slip factor and the magnetic field applied transversely are described as:

$$B(X,t) = B_0\left(\frac{X^{n-1}}{(1-\lambda t)}\right)^{\frac{1}{2}}, \qquad N(X,t) = N_1\left(\frac{X^{n-1}}{(1-\lambda t)}\right)^{-\frac{1}{2}}. \tag{2.11}$$

By using Eqs (2.10) and (2.11), Eqs (2.2), (2.4) and (2.9) reduce to

$$f''' + \frac{n+1}{2}ff'' - nf'^2 - Mf' - A(f' + \frac{\eta}{2}f'') = 0, \tag{2.12}$$

$$\frac{1}{\mathrm{Pr_{eff}}}\theta'' + \frac{(n+1)}{2}f\theta' + \mathrm{Nb}\,\phi'\theta' + Nt\,\theta'^2 - \frac{A}{2}\eta\theta' + \mathrm{Ec}(f'')^2 + Q\theta = 0, \tag{2.13}$$

$$\phi'' + \frac{(n+1)}{2}\mathrm{Le}f\phi' + \frac{Nt}{\mathrm{Nb}}\theta'' - \frac{A\mathrm{Le}}{2}\eta\phi' + S_r\theta'' = 0. \tag{2.14}$$

The preliminary and border conditions (2.5) and (2.6) become:

$$\begin{cases} f(\eta)=0,\ f'(\eta)=1+\gamma f''(\eta),\ \theta(\eta)=1,\ \phi(\eta)=1 \text{ at } \eta=0, \\ f'(\eta)\to 0,\ \theta(\eta)\to 0,\ \phi(\eta)\to 0 \text{ as } \eta\to 0, \end{cases} \tag{2.15}$$

where

$$Nt=\frac{\tau D_T(T_w-T_\infty)}{T_\infty \nu}, \qquad M=\frac{\sigma B_0^2}{\rho a}, \qquad A=\frac{\lambda_1}{aX^{n-1}},$$

$$\mathrm{Pr}=\frac{\nu}{\alpha_m}, \qquad \mathrm{Le}=\frac{\nu}{D_B}, \qquad \mathrm{Ec}=\frac{u_w^2}{C_p(T_w-T_\infty)},$$

$$\mathrm{Nb}=\frac{\tau D_B\,(C_w-C_\infty)}{\nu}, \qquad R=\frac{16\sigma^* T_\infty^3}{3kk^*},$$

$$S_r=\frac{D_m k_T}{\nu T_m}\frac{T_w-T_\infty}{C_w-C_\infty}, \qquad \mathrm{Pr_{eff}}=\frac{\mathrm{Pr}}{(1+R)\,(a\nu)^{\frac{1}{2}}}.$$

The concerned engineering parameters C_{f_X}, Nu_X, and Sh_X are

$$C_{f_X}=\frac{2\tau_w}{\rho u_w^2(X,t)}, \qquad \mathrm{Nu}_X=\frac{Xq_w}{k(T_w-T_\infty)}, \qquad \mathrm{Sh}_X=\frac{Xq_m}{D_B(C_w-C_\infty)}, \tag{2.16}$$

where τ_w, q_w, and q_m are given as:

$$\tau_w=\mu\left(\frac{\partial u}{\partial Y}\right)_{Y=0}, \qquad q_w=-\left[\left(k+\frac{16\sigma T^3}{3k^*}\right)\frac{\partial T}{\partial Y}\right]_{Y=0}, \qquad q_m=-D_B\left(\frac{\partial C}{\partial Y}\right)_{Y=0}. \tag{2.17}$$

With the help of Eqs (2.10) and (2.17), Eq. (2.16) reduces to

$$C_{f_X}\mathrm{Re}_X^{1/2}=f''(0), \qquad \mathrm{Nu}_X\mathrm{Re}_X^{-1/2}=-(1+R)\theta'(0), \qquad \mathrm{Sh}_X\mathrm{Re}_X^{-1/2}=-\phi'(0), \tag{2.18}$$

where $\mathrm{Re}_X=\frac{u_w(X,t)X}{\nu}$.

3. Method of solution

The set of differential Eqs (2.12)–(2.14), which are nonlinear with boundary conditions (2.15), Runge-Kutta integration scheme with shooting technique is implemented and are resolved using the software MATLAB function "bvp4c". The variables are defined as:

$$y_1 = f, \quad y_2 = f', \quad y_3 = f'', \quad y_3' = f'', \tag{3.1}$$

$$y_4 = \theta, \quad y_5 = \theta', \quad y_5' = \theta'', \tag{3.2}$$

$$y_6 = \phi, \quad y_7 = \phi', \quad y_7' = \phi''. \tag{3.3}$$

By using (3.1), (3.2), and (3.3), Eqs (2.12)–(2.14) can be written as:

$$y_3' + \frac{n+1}{2} y_1 y_3 - n y_2^2 - M y_2 - A\left(y_2 + \frac{\eta}{2} y_3\right) = 0, \tag{3.4}$$

$$\frac{1}{\mathrm{Pr_{eff}}} y_5' + \frac{(n+1)}{2} y_1 y_5 + \mathrm{Nb}\, y_7 y_5 + N t\, y_5^2 - \frac{A}{2}\eta y_5 + \mathrm{Ec}(y_3)^2 + Q y_4 = 0, \tag{3.5}$$

$$y_7' + \frac{(n+1)}{2}\mathrm{Le}\, y_1 y_7 + \frac{Nt}{\mathrm{Nb}} y_5' - \frac{A\mathrm{Le}}{2}\eta y_7 + S_r y_5' = 0. \tag{3.6}$$

To solve the various problems related to boundary layer flows, this technique is successfully used. Insert initial guesses to $f''(0)$, $-\theta'(0)$ and $-\phi'(0)$ for approximate solution. Here the step size and convergence criteria are chosen to be 0.001 and 10^{-8} (in all cases).

4. Results

The solutions of the non-dimensional Eqs (2.12)–(2.14) with boundary conditions (2.15) are obtained by applying the numerical technique called the bvp4c function. Effects of various flow governing parameters over the nanofluid velocity, temperature and nanoparticle concentration has been determined. The values of engineering interests i.e., local skin friction coefficient, local Nusselt and Sherwood numbers have been computed for various regulatory parameters of flow field. All the outcomes are depicted in graphs for better perception. The work

Table 1. The values of $-\theta'(0)$ when Le = 10, $A = \gamma = R = \text{Ec} = \text{Sr} = M = Q = 0$, Pr = 10 and $n = 1$.

Nb	Nt	Khan and Pop [39]	Seth and Mishra [40]	Present result
0.1	0.1	0.9524	0.9526	0.9612
	0.2	0.6932	0.6934	0.7161
	0.3	0.5201	0.5212	0.5398
0.2	0.1	0.5056	0.5052	0.5137
	0.2	0.3654	0.3655	0.3700
	0.3	0.2731	0.2734	0.2819

Table 2. The values of $-\varphi'(0)$ when Le = 10, $A = R = \gamma = \text{Ec} = \text{Sr} = M = Q = 0$, Pr = 10 and $n = 1$.

Nb	Nt	Khan and Pop [39]	Seth and Mishra [40]	Present result
0.1	0.1	2.1294	2.1309	2.1651
	0.2	2.2740	2.2739	2.2834
	0.3	2.5286	2.5229	2.6213
0.2	0.1	2.3819	2.3867	2.4086
	0.2	2.5152	2.5181	2.6191
	0.3	2.6555	2.6556	2.6976

has been done numerically for all the considerations by implementing the defaulting values $A = 1$, $\text{Pr}_{\text{eff}} = 1$, $M = 0.5$, $n = 2$, $Nt = 0.2$, Le = 2, Nb = 0.2, and $\gamma = 0.1$, until otherwise specified particularly. To evaluate the code validity of the current method, a comparison is presented in Tables 1 and 2 for $-\theta'(0)$ and $-\phi'(0)$ values and Nb and Nt. There is a good agreement obtained using the present method.

The effects of various governing parameters n, A, M, γ, Pr, R, Le, Nt, Nb, Ec, Q, and Sr on $f''(0)$, $-\theta'(0)$ and $-\phi'(0)$ are shown in Table 3. In Table 3, it is noted that as n or A increase, $f''(0)$, $-\theta'(0)$ and $-\phi'(0)$ increase as well, whereas these decreases as γ increases. Physically, the slip parameter γ creates a resistive force near the stretching sheet, which reduces the friction factor as well as thermal and mass transfer rates. $f''(0)$ does not have effect on rising the values of Pr or R or Le or Nt or Nb or Ec or Q or Sr. A decrease in the $-\theta'(0)$ is observed as M or Le or Nt or Nb or Q increases and an increase in $-\theta'(0)$ is noted for rising values of Pr or R or Sr. It is noted that the heat transfer rate decreases with the increasing Ec, while a reversed trend is observed in the rate of mass transfer. In fact, the presence of Ec generates viscous heating that reduces the heat transfer rate at the surface of the moving plate. A decrease

Table 3. Numerical outcomes for $f''(0)$, $-\theta'(0)$ and $-\phi'(0)$ for various values of n, A, γ, Pr, R, Le, Nt, Nb, Ec, Q, M, Sr.

n	A	M	γ	Pr	R	Le	Nt	Nb	Ec	Q	Sr	$f''(0)$	$-\theta'(0)$	$-\phi'(0)$
5	1	0.5	0.1	0.7	0.2	2.0	0.5	0.5	0.02	0.5	0.1	1.8872	0.6750	1.1376.
6	1	0.5	0.1	0.7	0.2	2.0	0.5	0.5	0.02	0.5	0.1	1.9881	0.7358	1.3020
7	1	0.5	0.1	0.7	0.2	2.0	0.5	0.5	0.02	0.5	0.1	2.0793	0.7911	1.4485
5	2	0.5	0.1	0.7	0.2	2.0	0.5	0.5	0.02	0.5	0.1	1.9805	0.8398	0.6510
5	3	0.5	0.1	0.7	0.2	2.0	0.5	0.5	0.02	0.5	0.1	2.0690	0.9793	0.2114
5	1	1.0	0.1	0.7	0.2	2.0	0.5	0.5	0.02	0.5	0.1	1.9519	0.6559	1.0783
5	1	1.5	0.1	0.7	0.2	2.0	0.5	0.5	0.02	0.5	0.1	2.0131	0.6381	1.0213
5	1	0.5	0.5	0.7	0.2	2.0	0.5	0.5	0.02	0.5	0.1	0.9895	0.5159	0.6640
5	1	0.5	1.0	0.7	0.2	2.0	0.5	0.5	0.02	0.5	0.1	0.6379	0.4209	0.3585
5	1	0.5	0.1	1.0	0.2	2.0	0.5	0.5	0.02	0.5	0.1	1.8872	0.7772	1.1826
5	1	0.5	0.1	3.0	0.2	2.0	0.5	0.5	0.02	0.5	0.1	1.8872	0.8580	1.3904
5	1	0.5	0.1	0.7	0.5	2.0	0.5	0.5	0.02	0.5	0.1	1.8872	0.7568	1.1003
5	1	0.5	0.1	0.7	1.0	2.0	0.5	0.5	0.02	0.5	0.1	1.8872	0.8586	1.0337
5	1	0.5	0.1	0.7	0.2	3.0	0.5	0.5	0.02	0.5	0.1	1.8872	0.6605	1.5875
5	1	0.5	0.1	0.7	0.2	4.0	0.5	0.5	0.02	0.5	0.1	1.8872	0.6528	1.9547
5	1	0.5	0.1	0.7	0.2	2.0	1.0	0.5	0.02	0.5	0.1	1.8872	0.5871	0.9588
5	1	0.5	0.1	0.7	0.2	2.0	1.5	0.5	0.02	0.5	0.1	1.8872	0.5101	0.8465
5	1	0.5	0.1	0.7	0.2	2.0	0.5	1.0	0.02	0.5	0.1	1.8872	0.5492	1.2821
5	1	0.5	0.1	0.7	0.2	2.0	0.5	1.5	0.02	0.5	0.1	1.8872	0.4439	1.3143
5	1	0.5	0.1	0.7	0.2	2.0	0.5	0.5	0.04	0.5	0.1	1.8872	0.6662	1.1437
5	1	0.5	0.1	0.7	0.2	2.0	0.5	0.5	0.06	0.5	0.1	1.8872	0.6573	1.1497
5	1	0.5	0.1	0.7	0.2	2.0	0.5	0.5	0.02	1.0	0.1	1.8872	0.4149	1.2195
5	1	0.5	0.1	0.7	0.2	2.0	0.5	0.5	0.02	1.5	0.1	1.8872	0.0165	1.3047
5	1	0.5	0.1	0.7	0.2	2.0	0.5	0.5	0.02	0.5	0.2	1.8872	0.6770	1.1115
5	1	0.5	0.1	0.7	0.2	2.0	0.5	0.5	0.02	0.5	0.3	1.8872	0.6790	1.0851

in Sherwood number as R or Nt or Sr increases and an increase in Sherwood number for increasing Pr or Le or Nb or Ec or Q are observed.

The behavior of nanofluid velocity, temperature, and concentration profiles in the presence of unsteadiness parameter A are plotted in Figs 2, 3, and 4. It is observed that an increase in unsteadiness parameter A decreases the velocity and temperature of the fluid. In addition, both the momentum and thermal boundary layer thickness reduce for growing values of A. Physically, when unsteadiness increases the sheet loses heat and decline in the liquid temperature is noticed. Figure 4 shows that the concentration of the nano-particle and A are directly proportional.

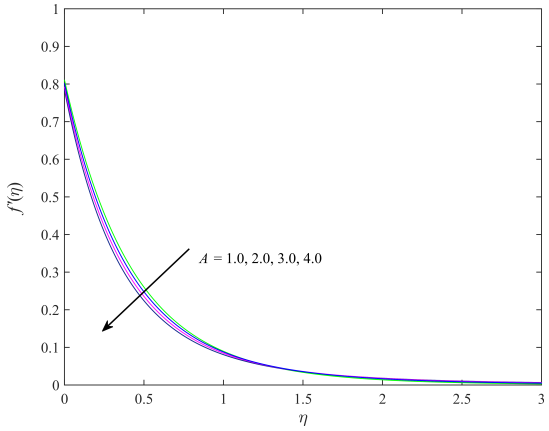

FIG. 2. Outcome of A on velocity.

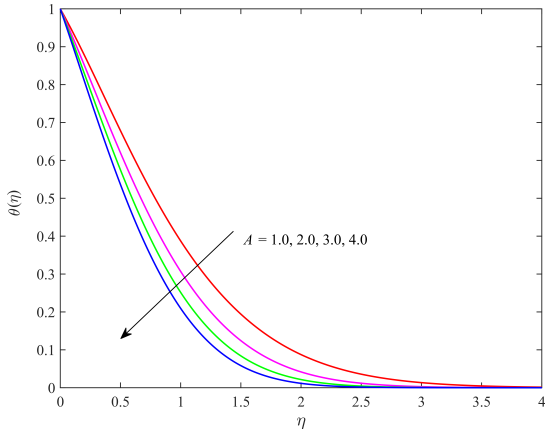

FIG. 3. Outcome of A on temperature.

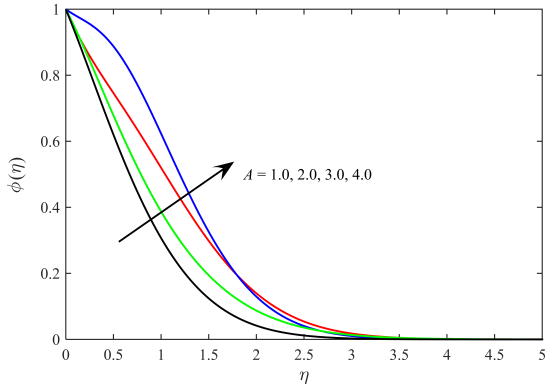

FIG. 4. Outcome of A on concentration.

Figures 5, 6, and 7 are plotted to study the behavior of nanofluid velocity, temperature and concentration profiles in the presence of slip parameter. It is seen that the velocity declines for larger values of γ. An increase in slip denotes an improved slide between the fluid and the exterior of the sheet. Thus only a partial

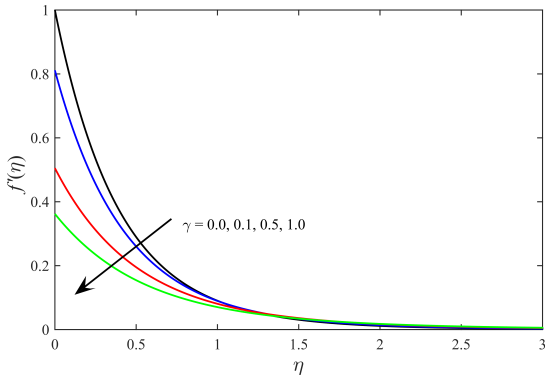

FIG. 5. Outcome of γ on velocity.

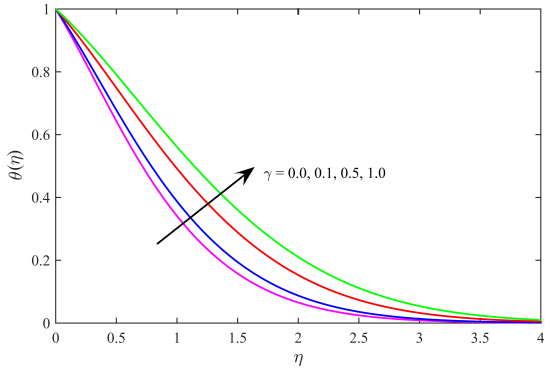

FIG. 6. Outcome of γ on temperature.

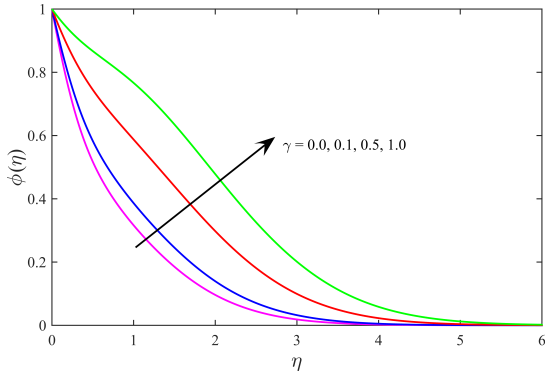

FIG. 7. Outcome of γ on concentration.

stretching velocity is transferred to the nanofluid resulting in a reduced velocity. The temperature and concentration increase as γ increases. It is observed in

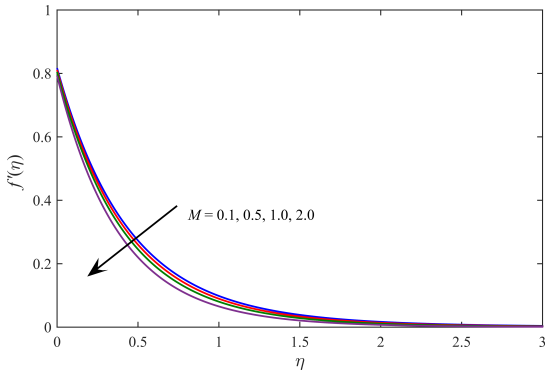

FIG. 8. Outcome of M on velocity.

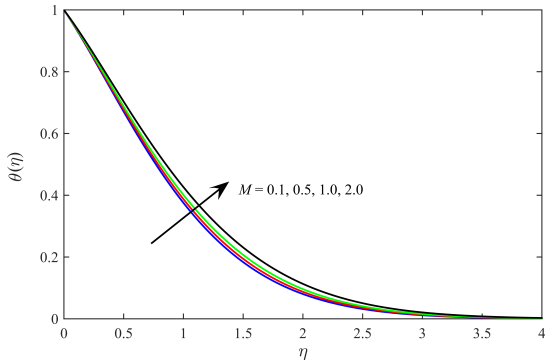

FIG. 9. Outcome of M on temperature.

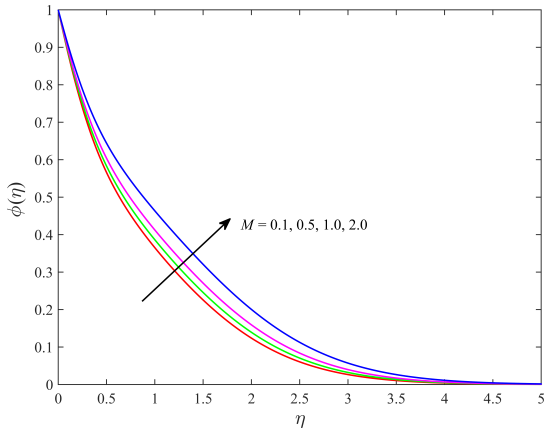

FIG. 10. Outcome of M on concentration.

Fig. 8 that as M increases the velocity declines. A resistance force called the Lorentz force is produced on the electrically conducting fluid by the application of a transverse magnetic field, which slows the fluid movement and shows a decrease in the velocity. As a result, an exterior magnetic field is a dominant means for managing the movement of the fluid. Figures 9 and 10 are plotted to study the effect of magnetic field M on a nanofluid temperature and concentration. The temperature and concentration both increase as M increases. The Lorentz force enhances the colliding nature of the molecules. This force accelerates the temperature in the thermal boundary layer, the concentration also increases.

The effect of Lewis number Le on the concentration profile is shown in Fig. 11. It is found that the nanoparticle concentration is a decreasing function of Le. Since stronger Lewis number intimates a weaker Brownian diffusion coefficient which result relatively small penetration depth for the concentration boundary layer. Figures 12, 13 and 14 illustrate that penetration depth of momentum, temperature and nanoparticle volume fraction decrease with the increasing values

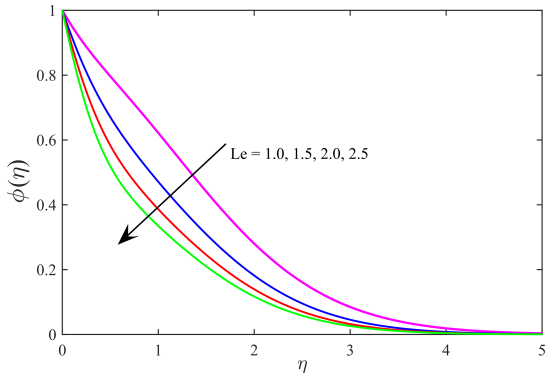

Fig. 11. Outcome of Le on concentration.

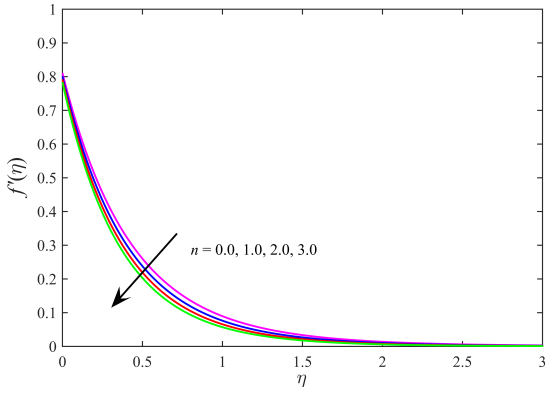

Fig. 12. Outcome of n on velocity.

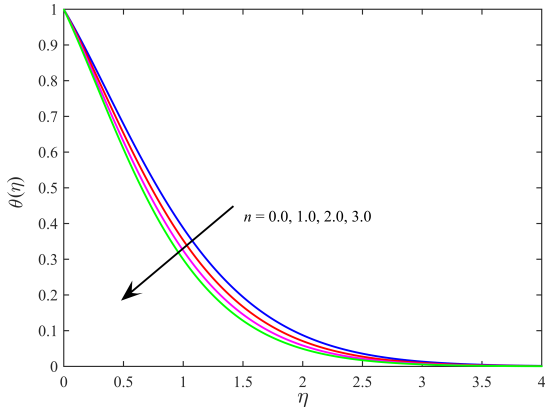

FIG. 13. Outcome of n on temperature.

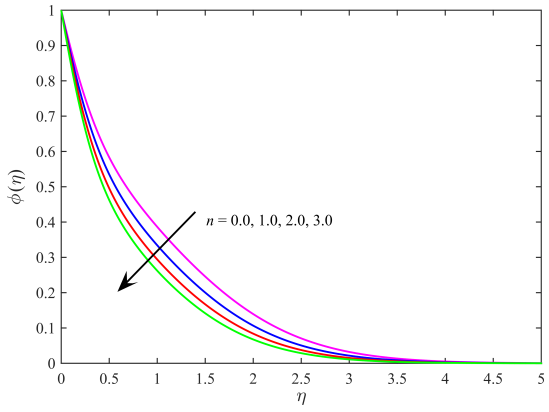

FIG. 14. Outcome of n on concentration.

of n, as n physically this is due to that fact that increase in power-law index n enhances the intensity of the cold fluid at the ambient towards the hot fluid in the vicinity of the sheet. This ultimately decreases the liquid temperature close to the stretching wall.

It is observed in Figs 15 and 16 that the temperature increases as Nb and Nt values increase. In view of physics, the strength of Nb strengthens the thermal conductivity of host fluid and the potency of Nt creates the thermophoretic force because of the temperature gradient, which sets off a speedy flow away from the sheet. Thus, the thermal boundary layer becomes thicker when the hot fluid is moved away from the surface. It is noticed from the figures that this behavior is in a good agreement with the study by BUONGIORNO [36]. Figure 17 is plotted to analyze the behavior of $\theta(\eta)$ for various values of Q. The temperature has increasing tendency with increasing value of Q. This is due to heat generation exists in the thermal boundary layer for positive values of Q (heat source) and,

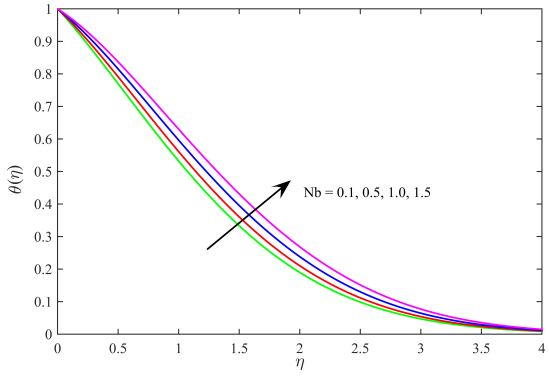

FIG. 15. Outcome of Nb on temperature.

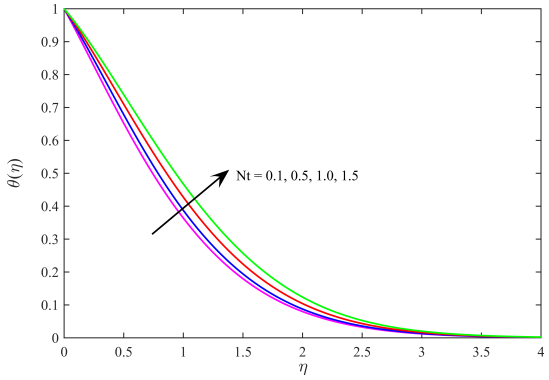

FIG. 16. Outcome of Nt on temperature.

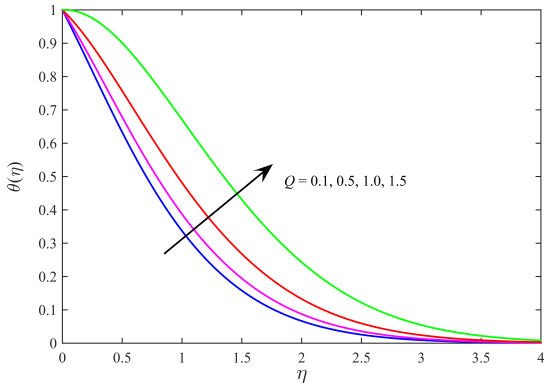

FIG. 17. Outcome of Q on temperature.

hence, temperature increases. The effect of Eckert number on temperature profile is plotted in Fig. 18. The Eckert number expresses the relationship between the

kinetic energy in the flow and the enthalpy. It embodies the conversion of kinetic energy into internal energy by work done against the viscous fluid stresses. The

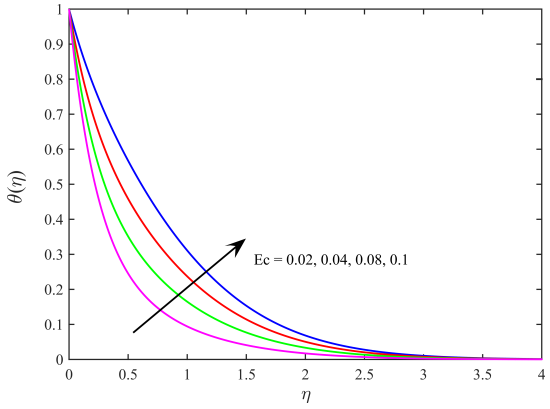

FIG. 18. Outcome of Ec on temperature.

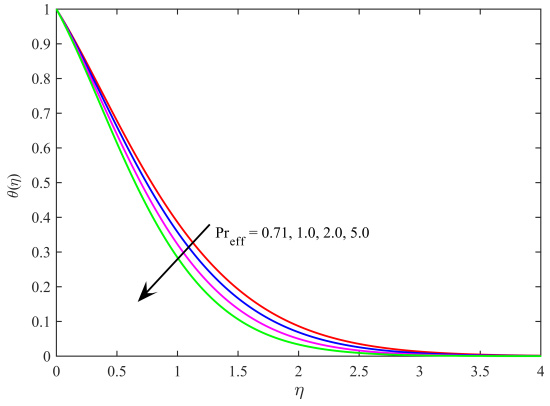

FIG. 19. Outcome of $\mathrm{Pr_{eff}}$ on temperature.

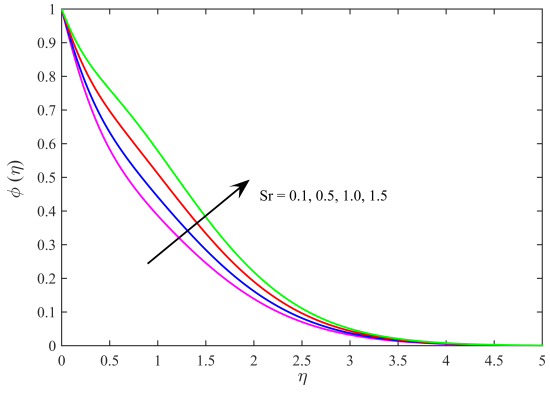

FIG. 20. Outcome of Sr on concentration.

effect of dissipation in the flow field is to increase the energy yielding a greater fluid temperature and, as a consequence, greater buoyancy force. The increase in the buoyancy force increases the temperature.

For a radiating fluid that is optically thick, the temperature is a function of Pr and R. Therefore, effective Pr, i.e., a combination of Pr and R on temperature has been marked in Fig. 19. It is noticed that for stronger $\mathrm{Pr}_{\mathrm{eff}}$ the temperature as well as the thickness of the thermal boundary layer decrease. The expression $\mathrm{Pr}_{\mathrm{eff}}$ says clearly that $\mathrm{Pr}_{\mathrm{eff}}$ and R are inverse to each other. Figure 20 outlines the concentration in the presence of the Soret number. An increase in Sr increases the concentration within the boundary layer and shows a strong effect on vertical boundary layer thickness.

5. Conclusions

A mathematical model has been presented with the Soret effect on MHD free convection nanofluid flow past an impulsively started nonlinear stretching sheet in the presence of thermal radiation, viscous dissipation and heat generation. The nanofluid momentum, temperature and concentration of a nanoparticle have been numerically evaluated by the MATLAB bvp4c solver. The findings are given below.

Nanofluid temperature increases for γ, Nb, Nt, Q, and except for the n and A it has a tendency to decrease. All the parameters A, γ, M, and n have the tendency to decline the nanofluid motion. The investigation reveals that concentration is an increasing function of velocity slip and the Soret number whereas it is decreasing function of Lewis number and the stretching index.

The general inference of the current effort is that the concentration of a nanoparticle is influenced by the Soret effect. Hence, the Soret effect assumes significance in the cases concerning isotope separation and in the mixtures between gases with very light molecular weight (H_2, He) and the medium molecular weight (N_2, air), the Soret effect cannot be ignored.

The problem of fluid flow past a stretching sheet has been considered in this paper. Based on the results obtained, we wish to study more complex transfer models such as flow along a curved surface of the cylinder, square cavity, needle, which are of more practical interest with different methods of solutions.

References

1. Choi S.U.S., Eastman J.A., *Enhancing thermal conductivity of fluids with nanoparticles*, Unites States, 1995.

2. Das Sk., Choi S.U.S., Wenhua Yu, Pradeep T., *Nanofluids: Science and Technology*, John Wiley & Sons, Inc., 2008.

3. Afridi M.I., Qasim M., Khan N.A., Hamdani M., Heat transfer analysis of Cu-Al_2O_3-water and Cu-Al_2O_3-kerosene oil hybrid nanofluids in the presence of frictional heating: using 3-stage Lobatto IIIA formula, *Journal of Nanofluids*, **8**(4): 885–891, 2019, doi: 10.1166/jon.2019.1626.

4. Afridi M.I., Tlili I., Goodarzi M., Osman M., Khan N.A., Irreversibility analysis of hybrid nanofluid flow over a thin needle with effects of energy dissipation, *Symmetry*, **11**(5): 663, 2019, doi: 10.3390/sym11050663.

5. Crane LJ., Flow past a stretching plate, *Journal of Applied Mathematics and Physics*, **21**(4): 645–647, 1970.

6. Mustafa M., Khan J.A., Model for flow of Casson nanofluid past a non-linearly stretching sheet considering magnetic field effects, *AIP Advances*, **5**(7): 1–11, 2015, doi: 10.1063/1.4927449.

7. Das K., Nanofluid flow over a non-linear permeable stretching sheet with partial slip, *Journal of the Egyptian Mathematical Society*, **23**(2): 451–456, 2015, doi: 10.1016/j.joems.2014.06.014.

8. Badr A., Subhas A.M., MHD boundary layer flow over a nonlinear stretching sheet in a nanofluid with convective boundary condition, *Journal of Computational and Theoretical Nanoscience*, **12**(12): 6020–6027, 2015, doi: 10.1166/jctn.2015.4753.

9. Rahman M.M., Eltayeb I.A., Radiative heat transfer in a Hydromagnetic nanofluid past a non-linear stretching surface with convective boundary condition, *Meccanica*, **48**(3): 601–615, 2013, doi:10.1007/s11012-012-9618-2.

10. Mustafa M., Khan J.A., Hayat T., Alsaedi A., Boundary layer flow of nanofluid over a nonlinearly stretching sheet with convective boundary condition, *IEEE Transactions on Nanotechnology*, **14**(1): 159–168, 2015, doi: 10.1109/TNANO.2014.2374732.

11. Hamad M.A.A., Pop I., Ismail A.M., Magnetic field effects on free convection flow of a nanofluid past a vertical semi-infinite flat plate, *Nonlinear Analysis: Real World Applications*, **12**(3): 1338–1346, 2011, doi: 10.1016/j.nonrwa.2010.09.014.

12. Bala Anki Reddy P., Suneetha S., Bhaskar Reddy N., Numerical study of MHD boundary layer slip flow of a Maxwell nanofluid over an exponentially stretching surface with convective boundary condition, *Propulsion and Power Research*, **6**(4): 259–268, 2017, doi: 10.1016/j.jppr.2017.11.002.

13. Daniel Y.S., Aziz Z.A., Ismail Z., Salah F., Effects of slip and convective conditions on MHD flow of nanofluid over a porous nonlinear stretching/shrinking sheet, *Australian Journal of Mechanical Engineering*, **16**(3): 1–17, 2017, doi: 10.1080/14484846.2017.1358844.

14. Hayat T., Ullah I., Alsaed I A., Farooq M., MHD flow of Powell-Eyring nanofluid over a non-linear stretching sheet with variable thickness, *Results in Physics*, **7**: 189–196, 2017, doi: 10.1016/j.rinp.2016.12.008

15. Uddin M.J., Sohail A., Anwar Bég O., Ismail A.I. Md., Numerical solution of MHD slip flow of a nanofluid past a radiating plate with Newtonian heating: A Lie group approach, *Alexandria Engineering Journal*, **57**(4): 2455–2462, 2018, doi: 10.1016/j.aej.2017.03.025.

16. Rana P., Dhanai R., Kumar L., Radiative nanofluid flow and heat transfer over a nonlinear permeable sheet with slip conditions and variable magnetic field: Dual solutions, *Ain Shams Engineering Journal*, **8**(3): 341–352, 2017, doi: 10.1016/j.asej.2015.08.016.

17. Lu D., Ramzan M., ul Huda N., Chung J. D., Farooq U., Nonlinear radiation effect on MHD Carreau nanofluid flow over a radially stretching surface with zero mass flux at the surface, *Scientific Reports*, **8**: 3709, 2018, doi:10.1038/s41598-018-22000-w.

18. Zaib A., Rashidi M.M., Chamkha A.J., Mohammad N.F., Impact of nonlinear thermal radiation on stagnation-point flow of a Carreau nanofluid past a nonlinear stretching sheet with binary chemical reaction and activation energy, *Proceedings of the Institution of Mechanical Engineers, Part C: Journal of Mechanical Engineering Science*, **232**(6): 962–972, 2018, doi: 10.1177/0954406217695847.

19. Magyari E., Pantokratoras A., Note on the effect of thermal radiation in the linearized Rosseland approximation on the heat transfer characteristics of various boundary layer flows, *International Communications in Heat and Mass Transfer*, **38**(5): 554–556, 2011, doi: 10.1016/j.icheatmasstransfer.2011.03.006.

20. Afify A.A., The influence of slip boundary condition on Casson nanofluid flow over a stretching sheet in the presence of viscous dissipation and chemical reaction, *Mathematical Problems in Engineering*, 1–12, Article ID 3804751, 2017, doi: 10.1155/2017/3804751.

21. Reddy C.S., Kishan N., MHD boundary layer flow of Casson nanofluid over a nonlinear stretching sheet with viscous dissipation and convective condition, *Journal of Nanofluids*, **5**(6): 870–879, 2016, doi: 10.1166/jon.2016.1271.

22. Khan U., Ahmed N., Asadullah M., Mohyud-Din S.T., Effects of viscous dissipation and slip velocity on two-dimensional and axisymmetric squeezing flow of Cu-water and Cu-kerosene nanofluids, *Propulsion and Power Research*, **4**(1): 40–49, 2015, doi: 10.1016/j.jppr.2015.02.004.

23. Navier C., Dissertation on the laws of fluid movement [in French: Memoire sur les lois du mouvement des fluids], *Memoires de l'Academie Royale des Sciences de l'Institut de France*, **6**: 389–440, 1823.

24. Shaw S., Kameswaran P.K., Sibanda P., Effects of slip on nonlinear convection in nanofluid flow on stretching surfaces, *Boundary Value Problems*, **2016**: 2, 2016, doi: 10.1186/s13661-015-0506-2.

25. Oyelakin I.S., Mondal S., Sibanda P., Unsteady Casson nanofluid flow over a stretching sheet with thermal radiation, convective and slip boundary conditions, *Alexandria Engineering Journal*, **55**(2): 1025–1035, 2016, doi: 10.1016/j.ae.j.2016.03.003.

26. Khan N.A., Sultan F., MHD flow of a Williamson fluid over an infinite rotating disk with anisotropic slip, *Journal of Engineering Physics and Thermophysics*, **92**(6): 1625–1636, 2019, doi:10.1007/s10891-019-02083-6.

27. Khan N.A., Naz F., Sultan F., Entropy generation analysis and effects of slip conditions on micropolar fluid flow due to a rotating disk, *Open Engineering*, **7**(1): 185–198, 2017, doi:10.1515/eng-2017-0025.

28. Ramya D., Srinivasa Raju R., Anand Rao J., Rashidi M.M., Boundary layer viscous flow of nanofluids and heat transfer over a nonlinearly isothermal stretching sheet in the presence of heat generation/absorption and slip boundary conditions, *International Journal of Nanoscience and Nanotechnology*, **12**(4): 251–268, 2016, http://www.ijnnonline.net/article_22934.html.

29. Suneetha S., Bhaskar Reddy N., Ramachandra Prasad V., Radiation and mass transfer effects on MHD free convective dissipative fluid in the presence of heat source/sink, *Journal of Applied Fluid Mechanics*, **14**(1): 107–113, 2011.

30. Reddy S.R.R., Anki Reddy P.B., Suneetha S., Magnetohydrodynamic flow of blood in a permeable inclined stretching viscous dissipation, non-uniform heat source/sink and chemical reaction, *Frontiers in Heat and Mass Transfer*, **10**(22): 2018, doi: 10.5098/hmt.10.22.

31. Eckert E.R.G., Drake R.M., *Analysis of Heat and Mass Transfer*, Mc-Graw Hill, New York, 1972.

32. Yirga Y., Shankar B., MHD Flow and heat transfer of nanofluids through a porous media due to a stretching sheet with viscous dissipation and chemical reaction effects, *International Journal for Computational Methods in Engineering Science and Mechanics*, **16**(5): 275–284, 2015, doi: 10.1080/15502287.2015.1048385.

33. Ram Reddy Ch., Murthy P.V.S.N., Rashad A.M., Chamkha Ali J., Soret effect on stagnation-point flow past a stretching/shrinking sheet in a nanofluid-saturated non-Darcy porous medium, *Special Topics & Reviews in Porous Media – An International Journal*, **7**(3): 229–243, 2016,doi: 10.1615/SpecialTopicsRevPorousMedia.v7.i3.20.

34. Mishra S.R., Baag S., Mohapatra D.K., Chemical reaction and Soret effects on hydromagnetic micropolar fluid along a stretching sheet, *Engineering Science and Technology,an International Journal*, **19** (4): 1919–1928, 2016, doi: 10.1016/j.jestch.2016.07.016.

35. Freidoonimehr N., Rashidi M.M., Mahmud S., Unsteady MHD free convective flow past a permeable stretching vertical surface in a nano-fluid, *International Journal of Thermal Sciences*, **87**: 136–145, 2015, doi: 10.1016/j.ijthermalsci.2014.08.009.

36. Buongiorno J., Convective transport in nanofluids, *ASME Journal of Heat Transfer*, **128**(3): 240–250, 2006, doi: 10.1115/1.2150834.

37. Rohni A.M., Ahmad S., Ismail A.I.M., Pop I., Flow and heat transfer over an unsteady shrinking sheet with suction in a nanofluid using Buongiorno's model, *International Communications in Heat and Mass Transfer*, **43**: 75–80, 2013, doi: 10.1016/j.icheatmasstransfer.2013.02.001.

38. Kuznetsov A.V., Nield D.A., Natural convective boundary-layer flow of a nanofluid past a vertical plate, *International Journal of Thermal Sciences*, **49**(2): 243–247, 2010, doi: 10.1016/j.ijthermalsci.2009.07.015.

39. Khan W.A., Pop I., Boundary-layer flow of a nanofluid past a stretching sheet, *International Journal of Heat and Mass Transfer*, **53**(11–12): 2477–2483, 2010, doi: 10.1016/j.ijheatmasstransfer.2010.01.032.

40. Seth G.S., Mishra M.K., Analysis of transient flow of MHD nanofluid past a non-linear stretching sheet considering Navier's slip boundary condition, *Advanced Powder Technology*, **28**(2): 375–384, 2017, doi:10.1016/j.apt.2016.10.008.

Received May 22, 2018; accepted version April 28, 2020.
